Molecular Cancer Therapeutics

Anti-KIT Monoclonal Antibody Treatment Enhances the Antitumor Activity of Immune Checkpoint Inhibitors by Reversing Tumor-Induced Immunosuppression

Andrew J. Garton[1], Scott Seibel[1,2], Lori Lopresti-Morrow[1,3], Linda Crew[1,4], Neal Janson[1], Sreekala Mandiyan[1], E. Sergio Trombetta[1,2], Shannon Pankratz[1], Theresa M. LaVallee[1,2], and Richard Gedrich[1,2]

Abstract

The receptor tyrosine kinase KIT is an established oncogenic driver of tumor growth in certain tumor types, including gastrointestinal stromal tumors, in which constitutively active mutant forms of KIT represent an actionable target for small-molecule tyrosine kinase inhibitors. There is also considerable potential for KIT to influence tumor growth indirectly based on its expression and function in cell types of the innate immune system, most notably mast cells. We have evaluated syngeneic mouse tumor models for antitumor effects of an inhibitory KIT mAb, dosed either alone or in combination with immune checkpoint inhibitors. Anti-KIT mAb treatment enhanced the antitumor activity of anti–CTLA-4 and anti–PD-1 mAbs, and promoted immune responses by selectively reducing the immunosuppressive monocytic myeloid-derived suppressor cell population and by restoring $CD8^+$ and $CD4^+$ T-cell populations to levels observed in naïve mice. These data provide a rationale for clinical investigation of the human KIT-specific mAb KTN0158 in novel immuno-oncology combinations with immune checkpoint inhibitors and other immunotherapeutic agents across a range of tumor types. *Mol Cancer Ther; 16(4); 671–80. ©2017 AACR.*

Introduction

KIT (c-KIT, CD117, stem cell factor receptor) is a member of the type III receptor tyrosine kinase family, whose structure comprises five extracellular immunoglobulin (Ig)-like domains, a single transmembrane domain, and intracellular kinase catalytic and regulatory domains (1). The ligand for KIT, stem cell factor (SCF), activates the receptor by binding to the second and third Ig-like domains, thereby inducing receptor homodimerization, autophosphorylation, and activation of downstream signaling pathways (2, 3). The identification of key interactions that contribute to receptor homodimerization within the fourth Ig-like domain (D4) of KIT suggested a novel approach to inhibit KIT function by targeting this region of the receptor (4), enabling structure-based design of KTN0158, a humanized anti-KIT IgG1 mAb. KTN0158 is currently undergoing human clinical trials in cancer patients (phase 1 study: NCT02642016).

Constitutive signaling downstream of mutant forms of KIT is an established mechanism driving the growth of a number of human tumors, including gastrointestinal stromal tumors (GIST), melanoma, mastocytosis, and mast cell leukemia (5). Several tyrosine kinase inhibitors (TKI) of KIT have demonstrated clinical benefit in KIT-driven GIST (6–8). Wild-type KIT expression has also been reported on a range of tumors and hematologic malignancies, but generally the evidence does not support KIT signaling in these cancers as an oncogenic driver (9, 10). However, KIT is also expressed on innate immune cells, including mast cells, in the tumor microenvironment of many types of human cancer (11–14), suggesting the potential for involvement of KIT in modulating the immune response in cancer (15). Several studies have implicated KIT-expressing mast cells as a factor promoting immunosuppression within the tumor microenvironment in the majority of solid tumors, suggesting that selectively targeting KIT may represent an approach to promote antitumor immunity in a broad range of tumor types (16–20).

The dramatic clinical success of immunotherapy targeting the T-cell checkpoint proteins CTLA-4 and PDL-1/PD-1 in multiple tumor types has triggered the search for additional novel immuno-oncology approaches that may be evaluated as monotherapies or in combination with these agents (21). Indeed, whereas subsets of patients derive dramatic survival benefit from immune checkpoint inhibitors, the majority of patients do not respond, and in some tumor types, the benefit has limited impact on survival (22–24). In melanoma patients treated with immune checkpoint inhibitors, high numbers of circulating monocytic myeloid-derived suppressor cells (M-MDSC) are associated with lower survival benefit (25, 26), suggesting that approaches to target M-MDSCs may represent novel combination strategies to enhance the efficacy of immune checkpoint inhibitors. Previous studies have implicated mast cells as positive regulators of MDSC function (27, 28), and involvement of KIT-dependent

Kolltan Pharmaceuticals Inc., New Haven, Connecticut.

Current addresses: [1]Kolltan Pharmaceuticals Inc., New Haven, Connecticut; [2]Celldex Therapeutics, New Haven, Connecticut; [3]Kleo Pharmaceuticals, New Haven, Connecticut; [4]Alexion Pharmaceuticals, New Haven, Connecticut.

Note: Supplementary data for this article are available at Molecular Cancer Therapeutics Online (http://mct.aacrjournals.org/).

Corresponding Author: Richard Gedrich, Celldex Therapeutics, 300 George Street, Suite 530, New Haven, CT 06511. Phone: 203 836 5360; E-mail: rgedrich@celldex.com

doi: 10.1158/1535-7163.MCT-16-0676

signaling in these effects has been suggested through genetic approaches (17, 29) and with inhibitors of KIT (30–32). In the present study, we have evaluated the effect of targeting KIT with an inhibitory mAb in combination with antibodies that target the clinically relevant CTLA-4 and PD-1 immune checkpoint proteins in syngeneic mouse tumor models. Our results demonstrate that treatment with an anti-KIT mAb profoundly reduces the immunosuppressive M-MDSC population of tumor-bearing mice, resulting in enhanced antitumor efficacy of immune checkpoint inhibitors. These data support future clinical evaluation of the human KIT-specific mAb KTN0158 in combination with anti–PD-(L)1, and/or anti–CTLA-4 mAbs for the treatment of a broad range of human cancers.

Materials and Methods

Antibodies and inhibitors

Antibodies used for determination of SCF concentrations were from R&D Systems (DY455). The assay was performed essentially according to the manufacturer's protocol except that the assay was adapted for detection by electrochemiluminescence using Streptavidin-Sulfotag (MSD, R32AD-5). Inhibitory antibodies used for *in vitro* and *in vivo* experiments were anti-mouse KIT (ACK2, Biolegend; isotype control antibody LTF-2, BioXcell), anti-human KIT (KTN0158, produced at Kolltan Pharmaceuticals), anti–CTLA-4 (UC10-4F10-11; BioXcell), and anti–PD-1 (RMP1-14; BioXcell). Small-molecule TKIs were obtained from Selleck (imatinib, S1026; nilotinib, S1033).

Cell culture

The Colon26 cell line was obtained from the NCI tumor cell line repository and was cultured for less than 6 months prior to use. CHO cells were stably transfected with expression vectors containing full-length cDNA constructs encoding KIT from human, monkey, dog, and mouse (NCBI accession numbers: NP_001087241, XP_001089071, AAP76390, and BC052457). Mouse mast cells were prepared from C57Bl/6 bone marrow cells (IQ Biosciences IQB-MBM202) as described in ref. 33, and were matured in culture for 4 weeks prior to assay. At this stage, the culture consisted of 95% to 99% mast cells as determined by flow cytometry analysis of cells costained with the mast cell markers anti-KIT and anti-FcεR1α. Mast cell activation was assayed as described in ref. 34 by quantitating the fractional release of β-hexosaminidase in response to SCF (100 ng/mL) in the presence of submaximal concentrations of cross-linked IgE, achieved by the addition of anti–DNP-IgE (500 ng/mL) and DNP-HSA (12.5 ng/mL). β-Hexosaminidase activity was determined in both culture supernatants and cell pellet lysates as described previously (35).

KIT phosphorylation assays

KIT phosphorylation was assessed in all cultured cell types using a 96-well sandwich immunosorbent assay format with electrochemiluminescent detection. Cells were serum-starved overnight and preincubated with inhibitors for 2 hours prior to addition of the appropriate SCF (100 ng/mL) for 10 minutes, followed by cell lysis. Species-appropriate SCF preparations were obtained from commercial sources: human SCF (R&D Systems; 255-SC/CF—used for both human and monkey KIT CHO cells), canine SCF (R&D Systems; 2278-SC/CF), mouse SCF (R&D Systems; 455-MC-050—used for mouse mast cells and mouse KIT CHO cells). KIT protein was captured for detection using species-appropriate anti-KIT antibodies that recognize human, monkey, and dog KIT (Biolegend; 104D2) or mouse KIT (Biolegend; 2B8); pY20-Sulfotag (MSD; R32AP-1) was used for detection of tyrosine phosphorylated KIT by electrochemiluminescence.

In vivo studies

In vivo studies, including flow cytometry analyses, were performed at Association for Assessment & Accreditation of Laboratory Animal Care–accredited contract research laboratories (Charles River Discovery Services, Colon26 model; Molecular Imaging Bioresearch, Pan02 model) under the guidance of the appropriate Institutional Animal Care and Use Committees. Tumor growth was monitored in two dimensions with calipers, and tumor size was estimated according to the formula: Tumor volume (mm^3) = (tumor width^2 × length)/2. Test articles were diluted in sterile PBS to achieve a fixed dosing volume of 0.2 mL (Colon26) or 0.1 mL (Pan02), and were administered i.p. to mice in groups of 10 (efficacy study) or 5 (flow cytometry studies).

Colon26 model. Colon26 cells maintained in culture were inoculated in PBS (5×10^5 cells in 0.1 mL) into the right flank of 8-week-old female Balb/c mice (Charles River; Balb/c AnNCrl). Dosing regimens for the efficacy study were as follows: timing of dosing refers to the number of days after tumor implantation: Anti–CTLA-4 and control IgG mAbs (5 mg/kg on day 8, 2.5 mg/kg on days 11 and 14); anti–PD-1 mAb (5 mg/kg on days 3, 6, 10, and 13), anti-KIT mAb (1, 3, 10, or 15 mg/kg on days 3, 6, 10, and 13). Tumor tissue was harvested for immunohistochemistry staining on day 22 from satellite animals dosed with control IgG. Tissue was preserved in 10% neutral-buffered formalin and stored at room temperature prior to preparation of paraffin blocks. Sections were stained with the mast cell–specific markers toluidine blue and mast cell tryptase, and representative images were collected and analyzed with Imagescope software (Version 12.2.2.5; Aperio).

Dosing for flow cytometry analysis was initiated 14 days after cell implant (tumor volume, 150–250 mm^3) and was performed on days 14 and 18 for all agents, using the same dose levels as in the tumor growth study (anti-KIT was administered only at the 15 mg/kg dose); tumor and spleen samples were collected on day 21. Tumors were processed for flow cytometry using the gentleMACS tumor dissociation Kit (Miltenyi Biotec), followed by processing with Histopaque-1077 (Sigma) to obtain tumor-infiltrating lymphocytes. Spleen samples were dissociated by grinding tissue in RPMI-1640 medium across mesh, followed by red blood cell lysis using ACK lysis buffer (Thermo-Fisher; A1049201). Cell suspensions were prepared for flow cytometry at 1×10^7 cells/mL in PBS (pH 7.4) containing 2.5% FBS and 0.09% NaN_3.

Pan02 model. Pan02 tumors were maintained *in vivo* by serial subcutaneous passage in female C57BL/6 mice (Harlan; C57BL/6NHsd). Study mice were implanted into the right axilla of C57BL/6 mice using an 11-gauge trocar needle with 30 to 50 mg fragments obtained from 750 mm^3 passage tumors. Dosing for flow cytometry analysis was initiated 14 days after cell implant (mean tumor volume, 186 mm^3) and was performed on days 14, 16, 18, and 20 for anti-KIT and control IgG (15 mg/kg), and on days 14 (5 mg/kg) and 17 (2.5 mg/kg) for anti–CTLA-4. Blood,

tumor, and spleen samples were collected on day 21. Blood was collected after CO_2 euthanasia by cardiac puncture, inverted in serum collection tubes (BD, Microtainer), and centrifuged; serum was then stored at −80°C until used. Spleens and tumors were processed for flow cytometry analysis as described for the Colon26 samples; final cell suspensions were prepared in flow cytometry staining buffer (R&D Systems; FC001).

Flow cytometry analysis

Flow cytometry was performed by standard methods using either FACSCanto II (BD; for Colon26 samples) or Attune NxT (Thermo Fisher; for Pan02 sample analysis) flow cytometers. Fc receptors were blocked by incubation with anti-CD16/CD32 (BD; 553142) prior to incubation with panels of fluorescent-labeled antibodies for staining of marker proteins to enable cell type identification and enumeration. Gating to select single cells was initially performed using FSC-H versus FSC-A plots, followed by exclusion of dead cells based on lack of staining with a dead cell stain [Colon26 study: Live/Dead Aqua (Life Technologies; L-34965); Pan02 study: Zombie NIR (BioLegend; 423105)]. Live single cells were then further segregated to identify $CD4^+$ T cells ($CD3^+CD4^+CD8^-$), $CD8^+$ T cells ($CD3^+CD4^-CD8^+$), M-MDSC ($CD3^-CD11b^+Ly6G^-Ly6C^{high}$), and G-MDSC ($CD3^-CD11b^+Ly6G^+Ly6C^{low}$). In the Pan02 study, CD45 staining was included as a first marker-specific gate to select leukocytes prior to subsequent gating for specific cell types; in addition, both CD3 and CD19 staining were used as exclusion gates for MDSC population analysis. Regulatory T cells (Treg) were also enumerated in the Pan02 study ($CD45^+CD3^+CD4^+CD25^+FoxP3^+$). Examples of flow cytometry gating plots used to identify each cell type are shown in Supplementary Fig. S1.

Graphing and data analysis

Graphing and data analysis, including IC_{50} determinations using a four-parameter nonlinear regression model, was performed using GraphPad Prism 6.05. Statistical analyses were also performed with GraphPad Prism using one-way ANOVA (flow cytometry analysis) or Mann–Whitney *U* test (Colon26 tumor growth analysis).

Results

Mammalian species selectivity of the anti-KIT mAb KTN0158 and characterization of ACK2 as a surrogate for studies in mouse models

KTN0158 is a humanized anti-KIT IgG1 mAb that is currently in clinical trials as a potential therapy for cancer. This antibody demonstrates potent inhibition of mammalian KIT in cells, with IC_{50} values of 169 pmol/L (human), 161 pmol/L (monkey), and 862 pmol/L (dog; Supplementary Fig. S2), but demonstrated no inhibition of mouse KIT at concentrations up to 1 μmol/L (Fig. 1A), indicating that, in order to assess the effects of selective inhibition of KIT by a mAb in syngeneic mouse tumor models *in vivo*, a surrogate antibody would be required. Potential surrogate antibodies were evaluated for their ability to inhibit mouse KIT phosphorylation and activity. The anti-KIT mAb ACK2 (36) inhibited mouse KIT phosphorylation in engineered cells with a mean IC_{50} value of 175 pmol/L (Fig. 1A), comparable with the potency of KTN0158 against human KIT. An isotype control antibody (LTF-2, rat IgG2b) had no effect on mouse KIT phosphorylation at concentrations up to 1 μmol/L,

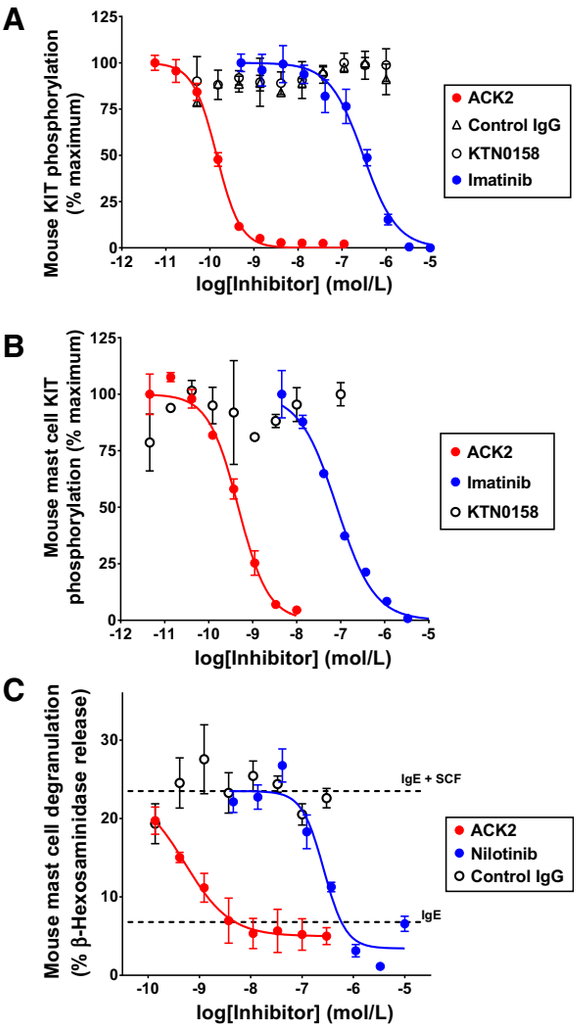

Figure 1.
Inhibition of mouse KIT by ACK2 in cell lines and primary mast cells. CHO cells engineered to overexpress mouse KIT (**A**), or cultured mouse mast cells that endogenously express KIT (**B**), were incubated with the indicated concentrations of KIT inhibitors or an isotype control IgG prior to stimulation with recombinant mouse SCF; lysates were then analyzed for KIT phosphorylation. Dose–response curves indicate the level of KIT phosphorylation relative to the maximum phosphorylation content (mean ± SD), and are representative examples from 2 to 13 replicate experiments. Mouse mast cells were sensitized to SCF-induced activation by preincubation with a submaximal concentration of cross-linked IgE. β-Hexosaminidase activity was assayed in both culture supernatants and cell pellets to determine the fraction released during degranulation (**C**). Data are plotted as the percentage of total cellular β-hexosaminidase released into the culture supernatant (mean ± SEM) and are representative of five replicate experiments. The dotted lines indicate the β-hexosaminidase released in control wells after treatment with cross-linked IgE alone or in the additional presence of SCF.

and therefore represents a useful negative control reagent for *in vivo* studies with ACK2 focused on the biological effects of KIT inhibition. ACK2 was also demonstrated to inhibit potently SCF-induced phosphorylation of endogenously expressed KIT on mouse mast cells (IC_{50} 290 pmol/L), whereas KTN0158, as

expected, had no effect (Fig. 1B). The functional impact of mouse KIT inhibition by ACK2 was also assessed by measuring β-hexosaminidase release during SCF-enhanced mast cell degranulation (37). ACK2 inhibited degranulation (Fig. 1C) with potency comparable with that of inhibition of SCF-induced KIT phosphorylation (IC_{50} 630 pmol/L). The isotype-matched control IgG had no effect in this system, whereas nilotinib, a TKI that inhibits KIT as well as Bcr-Abl, PDGFR, CSF-1R, and DDR (38), inhibited SCF-induced degranulation with an IC_{50} value of 303 nmol/L (Fig. 1C), consistent with previous reports (39). Taken together, these data indicate that ACK2 represents a suitable KTN0158 surrogate anti-KIT mAb with potency and biological properties appropriate for evaluation of the potential antitumor effects of KIT inhibition in mouse tumor models.

Expression and function of SCF/KIT in Colon26 tumor cells

The syngeneic mouse tumor model Colon26 is an established system for evaluation of novel immunotherapeutic approaches (40) which have been reported previously to express SCF (41). However, Colon26 cells grown *in vitro* did not express high levels of KIT protein as determined by immunoblotting or flow cytometry analysis (data not shown). The potential contribution of SCF/KIT-dependent signaling to proliferation of Colon26 cells was evaluated directly *in vitro* under standard or low-serum growth conditions, but no evidence for SCF-stimulated growth was observed (Supplementary Fig. S3). Furthermore, neither the anti-mouse KIT mAb ACK2 nor imatinib significantly affected cell growth, regardless of the culture conditions or presence/absence of SCF, indicating that KIT-driven signaling does not play a major role in proliferation of this cell line.

Antitumor activity of an anti-KIT mAb in combination with immune checkpoint inhibitors in the Colon26 mouse tumor model

The expression of SCF by Colon26 cells suggests the possibility of indirect effects on tumor growth via inhibition of KIT signaling on innate immune cells within the tumor microenvironment. KIT-expressing mast cells have been reported to infiltrate both human tumors and mouse tumor models (11, 28, 42), and mast cells were readily identified within established Colon26 tumor tissue in this study (Fig. 2A),

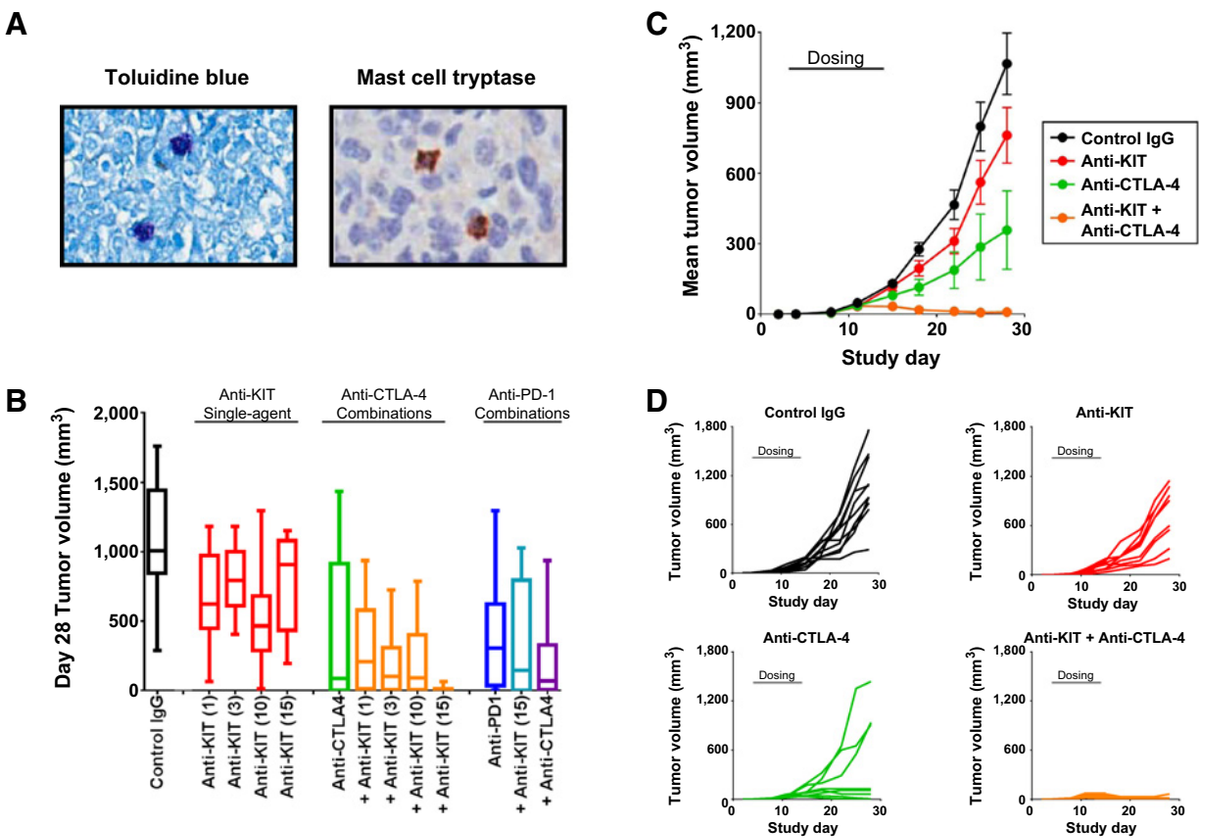

Figure 2.

Anti-KIT mAb enhances efficacy of immune checkpoint inhibitors in the Colon26 syngeneic mouse tumor model. Colon26 tumors harvested on day 22 after implant were stained with mast cell–specific markers toluidine blue and mast cell tryptase (**A**). Colon26 tumor cells were implanted into Balb/c mice, and groups of 10 mice were dosed with each of the indicated treatments as described in the Materials and Methods section. Tumor size at day 28 is shown as a box and whisker plot (**B**) indicating group median, 25th and 75th percentiles, minimum and maximum values for all study groups; anti-KIT mAb dose levels (mg/kg) are indicated in parentheses in the *x* axis labels. Tumor growth curves are also plotted for selected groups as group mean values ± SEM (**C**) and as individual tumor growth curves (**D**); in **C** and **D,** the anti-KIT mAb-containing dose groups are those that received 15 mg/kg anti-KIT mAb.

Table 1. Efficacy of anti-KIT mAb treatment in combination with immune checkpoint inhibitors in the Colon26 mouse tumor model

Treatment group	Median tumor size (mm^3)	Significance (vs. control IgG)	Number of tumors <50 mm^3 (day 28)	Number of late regressions	Number of tumor-free survivors (day 28)	Maximum body weight loss (%)
Control IgG	1,008	n/a	0	0	0	0
Anti–PD-1	305	<0.01	3	2	1	0
Anti–CTLA-4	86	<0.01	4	5	3	0
Anti–CTLA-4 + Anti–PD-1	69	<0.001	4	6	2	0
Anti-KIT (1)	625	ns	0	1	0	0
Anti-KIT (3)	794	ns	0	0	0	0
Anti-KIT (10)	466	<0.01	1	1	0	0
Anti-KIT (15)	908	ns	0	0	0	0
Anti–CTLA-4 + Anti-KIT (1)	209	<0.001	3	3	1	0
Anti–CTLA-4 + Anti-KIT (3)	104	<0.001	5	5	2	0
Anti–CTLA-4 + Anti-KIT (10)	92	<0.001	5	5	2	0
Anti–CTLA-4 + Anti-KIT (15)	0	<0.001	7	7	6	[a]8
Anti–PD-1 + Anti-KIT (15)	146	<0.01	5	5	3	0

NOTE: The Colon26 tumor model was evaluated for sensitivity to the indicated therapeutic agents in groups of 10 animals, and potential readouts of efficacy and tolerability are summarized. Tumor measurements were taken at day 28, following completion of the dosing phase when the control group tumors reached the predetermined maximum allowable size (mean tumor volume, 1,000 mm^3). Late regressions refer to the number of animals within a group in which, following the cessation of dosing, tumors demonstrated a reduced size in at least two consecutive measurements; tumor-free survivors are animals that were alive at the end of the study with no measurable tumor burden; maximum body weight loss is the maximum group mean body weight loss during the study relative to the group mean body weight prior to the dosing period. Statistical significance was determined as described in Materials and Methods based on tumor volumes at the study endpoint (day 28). Numbers in parentheses indicate the dose (mg/kg) of anti-KIT mAb.

Abbreviation: ns, no significant difference from the control treatment group.

[a]One treatment-related death (cause unknown) occurred in this treatment group (study day 17).

although the numbers of mast cells observed in different areas within these samples were quite variable (from less than 1% of the cells to approximately 5%). The ability of anti-KIT mAb treatment to impact tumor growth *in vivo* was evaluated at multiple dose levels in the Colon26 model, both in single-agent regimens and in combination with antibodies targeting the key T-cell checkpoint proteins CTLA-4 and PD-1. These reagents are potent inhibitors of mouse CTLA-4 and PD-1 (43, 44), and as such represent surrogates of the clinically validated immuno-oncology agents against human CTLA-4 (ipilimumab) and PD-1 (nivolumab, pembrolizumab) which have shown remarkable efficacy in multiple clinical indications (21). Dosing was initiated at day 3 after implant of the tumor cells to enable optimal exposure of infiltrated immune cell populations to systemically administered mAbs. In general, all treatment regimens were well-tolerated, whether as single agents or in combinations, based on the minimal effect of treatments on animal body weights (Table 1). All animals in the control IgG-dosed group developed tumors during the course of the study, although growth rates of individual tumors were variable (size range at day 28 was 288–1,764 mm^3). Statistical analysis of tumor sizes at day 28 with the Mann–Whitney *U* test indicated that all treatments resulted in statistically significant antitumor activity (P values <0.05 to <0.001), with the exception of the 1, 3, and 15 mg/kg single-agent anti-KIT dose groups (Table 1). Furthermore, the combination of a range of doses of anti-KIT mAb (1–15 mg/kg) with anti–CTLA-4 mAb yielded dose-dependent enhanced antitumor activity relative to monotherapy comparator groups ($P < 0.05$ at the highest anti-KIT dose level), including increased numbers of tumors with minimal size at day 28, and increased numbers of tumors that regressed following an initial period of outgrowth (Table 1; Fig. 2; Supplementary Fig. S4). These data suggest that the combination of anti-KIT and anti–CTLA-4 mAbs may represent a promising new combination for evaluation in cancer patients. The combination of anti-KIT mAb with anti–PD-1 mAb also demonstrated reduced tumor growth relative to the single-agent dose groups, although this effect was not statistically significant (Table 1; Fig. 2B). This combination also increased the number of animals exhibiting minimal or no measurable tumor burden at the end of the study (Table 1; Supplementary Fig. S4), suggesting that anti-KIT/anti–PD-1 mAbs may also be worth exploring as a novel immuno-oncology combination.

Taken together, these data suggest that selectively targeting KIT with a mAb *in vivo* promotes the antitumor activity of both PD-1 and CTLA-4–directed immune checkpoint inhibitors, presumably via effects on KIT-expressing innate immune cells whose impact on tumor growth may be mediated through potentiating the antitumor response of the adaptive immune system.

Anti-KIT mAb treatment specifically reduces the number of M-MDSCs

In order to investigate possible mechanisms for the enhanced antitumor effects of anti-KIT mAb when combined with anti–PD-1 and anti–CTLA-4 mAbs, intratumoral and splenocyte immune cell populations were quantitated by flow cytometry of samples harvested from dosed Colon26 tumor–bearing animals. Among the cell types evaluated, in both tumor and spleen samples, M-MDSCs were considerably reduced in number in all anti-KIT mAb-treated groups (i.e., single-agent and combination treatment groups) relative to the control IgG, anti–CTLA-4, and anti–PD-1-treated groups (Table 2; Fig. 3A and B). These data suggest that the enhanced antitumor effect observed when an anti-KIT mAb is combined with anti–CTLA-4 or anti–PD-1 mAbs may result from the reduced numbers of M-MDSCs, which would be expected to reduce immune response suppression indirectly via influencing the function of other immune cell types (45). Because anti-KIT mAb treatment alone was insufficient to generate a prominent antitumor response against the Colon26 model, it appears that the reduction in M-MDSC numbers following anti-KIT mAb treatment may be permissive but not sufficient for an effective antitumor

Table 2. Immune cell populations in mice following treatment with anti-KIT mAb and immune checkpoint inhibitors

Tumor model	Tissue	Treatment group	M-MDSC	M-MDSC *P* value	G-MDSC	$CD4^+$ T cells	$CD8^+$ T cells	Treg
Colon26	Tumor-infiltrating lymphocytes	Control IgG	6.16 ± 2.74	n/a	6.76 ± 3.08	9.29 ± 3.34	8.48 ± 6.49	nd
		Anti–CTLA-4	8.38 ± 2.79	ns	7.58 ± 5.76	15.20 ± 4.53	21.08 ± 14.96	nd
		Anti-PD-1	5.74 ± 1.52	ns	9.88 ± 3.35	15.51 ± 7.69	15.64 ± 8.78	nd
		Anti–CTLA-4 + Anti–PD-1	8.68 ± 2.41	ns	9.54 ± 2.11	13.36 ± 0.69	**31.88 ± 14.30	nd
		Anti-KIT	0.69 ± 0.27	<0.001	**14.6 ± 3.78	10.63 ± 1.94	10.24 ± 2.71	nd
		Anti-KIT + Anti–CTLA-4	1.42 ± 0.68	<0.01	11.18 ± 2.67	**19.80 ± 5.65	23.30 ± 7.13	nd
		Anti-KIT + Anti-PD-1	1.17 ± 0.67	<0.01	7.42 ± 1.69	*18.32 ± 2.84	20.72 ± 8.60	nd
	Splenocytes	Control IgG	1.87 ± 0.58	n/a	9.09 ± 1.73	18.08 ± 1.49	7.63 ± 0.75	nd
		Anti–CTLA-4	1.67 ± 0.45	ns	8.15 ± 3.77	19.08 ± 2.31	8.36 ± 1.48	nd
		Anti-PD-1	1.72 ± 0.16	ns	9.24 ± 1.42	19.62 ± 1.41	7.39 ± 0.48	nd
		Anti–CTLA-4 + Anti–PD-1	2.88 ± 0.79	<0.01	9.45 ± 3.85	19.72 ± 1.92	8.88 ± 0.82	nd
		Anti-KIT	0.20 ± 0.06	<0.0001	5.28 ± 0.96	*21.78 ± 0.60	8.13 ± 0.78	nd
		Anti-KIT + Anti–CTLA-4	0.20 ± 0.08	<0.0001	5.61 ± 3.48	**23.22 ± 3.75	8.42 ± 1.50	nd
		Anti-KIT + Anti-PD-1	0.20 ± 0.04	<0.0001	*4.26 ± 0.53	*22.32 ± 1.46	8.99 ± 0.65	nd
Pan02	Tumor-infiltrating lymphocytes	Control IgG	25.87 ± 5.18	n/a	4.10 ± 1.15	2.43 ± 0.34	6.04 ± 2.68	0.78 ± 0.22
		Anti–CTLA-4	24.95 ± 4.73	ns	5.10 ± 2.47	3.15 ± 1.01	6.44 ± 2.38	0.87 ± 0.38
		Anti-KIT	16.69 ± 3.24	<0.01	3.85 ± 1.20	3.08 ± 1.23	7.35 ± 3.60	0.80 ± 0.21
		Anti-KIT + Anti–CTLA-4	13.70 ± 3.22	<0.001	3.53 ± 1.34	3.28 ± 0.56	7.57 ± 1.11	0.87 ± 0.37
	Splenocytes	Naïve mice	5.16 ± 1.12	<0.0001	10.11 ± 2.01	*18.07 ± 1.44	***18.71 ± 0.35	*2.47 ± 0.46
		Control IgG	11.00 ± 1.95	n/a	12.04 ± 2.89	14.81 ± 0.95	12.62 ± 1.46	1.85 ± 0.23
		Anti–CTLA-4	12.73 ± 1.56	ns	15.06 ± 1.71	12.56 ± 1.76	11.72 ± 2.36	1.64 ± 0.23
		Anti-KIT	3.98 ± 1.48	<0.0001	10.99 ± 3.28	**18.57 ± 2.08	**18.17 ± 1.33	2.33 ± 0.27
		Anti-KIT + Anti–CTLA-4	3.90 ± 1.27	<0.0001	9.08 ± 0.91	**18.46 ± 1.38	*17.24 ± 3.84	**2.82 ± 0.39

NOTE: Immune cell populations were enumerated by flow cytometry in tumor and spleen samples harvested from tumor-bearing mice following treatment with the indicated agents. Values represent mean ± SD ($n = 5$) of each cell type as a percentage of total live cells. *P* values were obtained from comparison of treatment groups (and naïve mice groups) with the control IgG-dosed tumor-bearing animal group, and are reported in column 5 for M-MDSC's, or as asterisks in columns 6 to 9 for all other cell types (*, $P < 0.05$; **, $P < 0.01$; ***, $P < 0.001$; ****, $P < 0.0001$); all other values were not significantly different from the control group ($P > 0.05$). Abbreviations: n/a, not applicable; nd, not determined; ns, not significant ($P > 0.05$).

immune response, such that an enhanced response can be triggered by concomitant inhibition of the CTLA-4 or PD-1 checkpoint molecules.

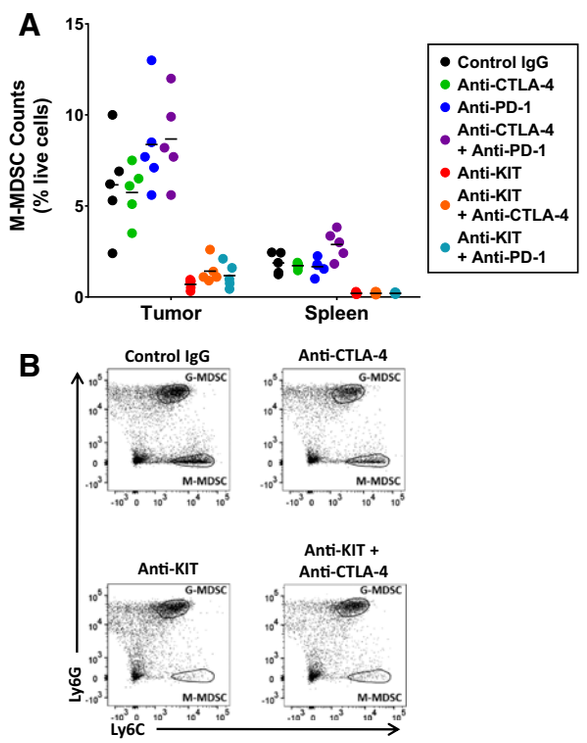

In order to explore further the generality of the effects observed in the Colon26 model, the effects of dosing with anti-KIT and anti–CTLA-4 mAbs were evaluated in the Pan02 pancreatic cancer model system. Pharmacokinetic analyses indicated that a more frequent dosing regimen would yield sustained exposure of the anti-KIT mAb in mice (data not shown). Therefore, in this study, the dosing frequency was increased (anti-KIT mAb was dosed every 48 hours) in order to maximize the impact of KIT inhibition on pharmacodynamic readouts of immune system function. The pharmacodynamic effects of anti-KIT and anti–CTLA-4 mAb treatment on circulating SCF concentrations were also measured. It has been reported previously that either genetic ablation of mouse KIT or treatment with TKIs results in compensatory increases in circulating SCF levels (46, 47). In mice dosed with anti-KIT mAb, either as a single agent or in combination with anti–CTLA-4 mAb, statistically significant ($P < 0.001$) increases in serum SCF concentrations relative to the control group were observed (Fig. 4A). Following dosing with anti–CTLA-4 mAb, serum SCF concentrations were unchanged from those in the control group. The magnitude of this increase in circulating SCF in anti-KIT mAb-treated mice was approximately 3-fold, which is comparable with that reported for KIT-deficient W/W^v mice relative to wild-type KIT littermates (47), indicating that the

Figure 3.
Anti-KIT MAb treatment decreases M-MDSC counts in Colon26 tumor-bearing mice. The M-MDSC population was enumerated by flow cytometry of single-cell suspensions prepared from tumor tissue or spleens of mice bearing Colon26 tumors (**A**); data represent the mean and individual values for each treatment group ($n = 5$). Representative flow cytometry scatter plots identifying the M-MDSC and G-MDSC populations are also shown (**B**).

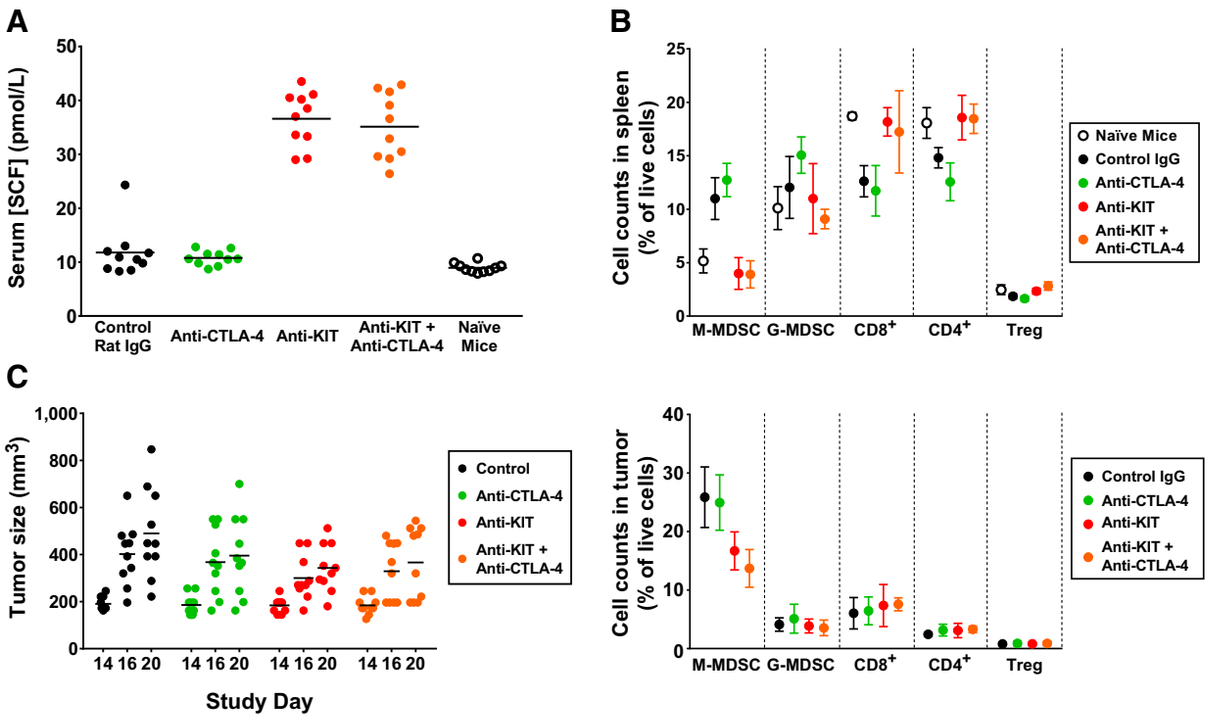

Figure 4.

Pharmacodynamic effects of anti-KIT and anti–CTLA-4 mAbs in the Pan02 syngeneic mouse tumor model. Serum SCF concentrations were determined by quantitative ELISA in Pan02 tumor–bearing mice and naïve control animals following dosing with the indicated agents (**A**); data plotted are mean and individual animal values (10 per group). Immune cell populations were enumerated by flow cytometry (**B**) in spleen (top) or tumor (bottom) samples from mice bearing Pan02 tumors, as well as spleen samples from naïve mice; data plotted are mean ± SD for each treatment group ($n = 5$). Pan02 tumor sizes were measured on days 14, 16, and 20 and are plotted as individual data points ($n = 10$) and mean group values (**C**).

anti-KIT mAb treatment regimen applied here was sufficient to substantially inhibit KIT function during the course of the study.

As previously reported by others (48), flow cytometric analyses indicated that the Pan02 model promoted a statistically significant increase ($P < 0.0001$) in the splenocyte M-MDSC population relative to naïve, non–tumor-bearing mice (Table 2; Fig. 4B, top). Furthermore, Pan02 tumor–bearing mice also exhibited suppressed splenocyte T-cell numbers relative to naïve mice, including reduced $CD4^+$ T cells, $CD8^+$ T cells, and Tregs, suggesting that this effect on the M-MDSC population is associated with functional immunosuppressive consequences (Table 2; Fig. 4B, top). Treatment of Pan02 tumor–bearing mice with anti-KIT as a single agent or in combination with anti–CTLA-4 significantly reduced the M-MDSC cell count in both spleen and tumor tissue relative to the control tumor-bearing group, and splenocyte M-MDSC numbers were reduced to the levels observed in naïve mice (Table 2; Fig. 4B). Furthermore, the numbers of splenocyte $CD4^+$ T-cell, $CD8^+$ T-cell, and Treg populations were also normalized (increased to levels observed in naïve mice) by anti-KIT mAb-containing treatment regimens (Table 2; Fig. 4B, top). Similar trends were observed in splenocyte $CD4^+$ and $CD8^+$ T-cell numbers in the anti-KIT treatment groups in the Colon26 model, although some of these changes failed to reach statistical significance (Table 2), supporting the notion that anti-KIT mAb treatment has the potential to affect tumor growth across model systems and histotypes by functionally affecting a variety of key immune cell types. Within the Pan02 tumor tissue, the only statistically significant effect observed across all dose groups was the reduction in M-MDSC numbers in both the anti-KIT single agent and anti-KIT + CTLA-4 combination group, which mirrored the observations in the Colon26 model (Table 2; Fig. 4B, bottom). There was no significant effect of anti-KIT mAb treatment on granulocytic myeloid-derived suppressor cell (G-MDSC) counts, or on the T-cell populations evaluated within the tumor tissue. Furthermore, treatment with anti–CTLA-4 mAb alone had no effect on any of the immune cell populations evaluated. Pan02 tumor growth during this study was also noticeably reduced by the combined treatment with anti-KIT and anti–CTLA-4, in that an increased number of tumors demonstrated minimal growth during the dosing period relative to the other dose groups (Fig. 4C).

Taken together, the data generated in two different syngeneic mouse tumor models suggest that anti-KIT mAb treatment has the potential to impact the sensitivity of multiple tumor types to immune checkpoint inhibitors via reducing suppression of the immune system, and that these effects may arise as a result of the profound reduction in M-MDSC numbers observed in spleen and tumor tissues. Studies to explore further the mechanism of action of anti-KIT mAb-enhanced responses to immune checkpoint inhibitors are ongoing.

Discussion

The critical role of MDSC populations in limiting antitumor immune responses is increasingly apparent, and identification of

novel approaches to target MDSC populations has therefore become a key goal for new cancer therapeutics discovery (49). In fact, in immunotherapy-treated human melanoma cancer patients, a prognostic relationship has been reported between low monocytic MDSC (M-MDSC) numbers and enhanced clinical benefit achieved with anti–CTLA-4 and anti–PD-1 immune checkpoint inhibitors (25, 26). Our results suggest that the combination of an immune checkpoint inhibitor with an inhibitory KIT-specific mAb has the potential to yield enhanced antitumor activity, as a consequence of reducing the numbers of M-MDSCs. Surprisingly, despite the expression and key role of KIT in a variety of immune cell types, including hematopoietic progenitor cells, this reduction in M-MDSC numbers in preclinical models appears to be relatively cell type specific because no reductions in G-MDSCs, $CD4^+$, or $CD8^+$ T cells or Treg populations were observed. In fact, increased cell numbers were observed in both the $CD4^+$ and $CD8^+$ T-cell populations within the splenocyte compartment, effectively normalizing the numbers of these cell types to the levels observed in naïve, non–tumor-bearing mice and potentially contributing to the antitumor activity of anti-KIT mAb treatment. These data suggest that the effects of treatment with a KIT antibody *in vivo* are not the result of general suppression of hematopoiesis and are more likely to reflect a specific role of KIT in modulating the immune system.

The effect of anti-KIT treatment on multiple immune cell populations within the splenocyte compartment supports the notion that KIT plays a relatively broad role in regulating tumor immunity, by affecting immune cell populations systemically as well as within the tumor tissue itself. The observation that anti-KIT increased $CD8^+$ and $CD4^+$ T-cell numbers in splenocytes but not in tumor-infiltrating lymphocytes was somewhat surprising because reduced M-MDSC numbers were observed in both tissues. It is possible that this apparent difference between spleen and tumor tissues reflects kinetic aspects of these experiments, such that changes in immune cell populations might be observed with different time courses in different compartments. Indeed, the percentage change in M-MDSC numbers following anti-KIT treatment was also greater in the splenocyte compartment (64% decrease) than in the tumor tissue (35% decrease; Table 2). Future studies evaluating the effects of anti-KIT treatment on the functional properties of tumor-infiltrating immune cell types will also be necessary in order to understand fully the mechanism of anti–KIT-enhanced tumor immunity.

Previous studies have suggested a potential role of mast cell KIT in suppression of immune responses in mouse models and human tumors, including the possibility that these effects occur via functionally modulating MDSCs. Genetic approaches in mast cell–deficient mice expressing mutant forms of KIT have demonstrated reduced tumor growth and metastasis relative to wild-type KIT-expressing mice, and adoptive transfer studies suggest a potential role for mast cells in these effects (16–18). Additional studies have highlighted mast cell–mediated effects on MDSCs as a potential mechanism underlying enhanced antitumor immune responses via modulating mast cell function (27, 28, 32). The impact of KIT inhibition on antitumor responses has also been evaluated using TKIs, demonstrating enhanced antitumor immune responses together with modified immune cell populations including reduced MDSCs (30, 31, 50–52). Whereas these molecules recognize a number of kinase targets in addition to KIT, each of which may contribute to any observed immune cell changes, these studies together with our observations strongly support clinical evaluation of an anti-KIT mAb in combination with immune checkpoint inhibitors. The therapeutic potential of selective KIT inhibition as a mechanism for enhancing immune responses was evaluated previously in the MCA26 model by combining the anti-KIT mAb ACK2 with a T-cell costimulatory receptor antibody (anti–4-1BB) and a recombinant IL12-expressing adenovirus (32). This study demonstrated enhanced antitumor efficacy when all three agents were combined, indicating that anti-KIT mAbs have the potential to enhance antitumor immunity in combination with experimental immunotherapeutic agents acting through diverse mechanisms, and supporting broad clinical evaluation of anti-KIT mAb immunotherapy combinations. In addition, enhanced MDSC function and infiltration into tumor tissue were observed in an RNAi-generated, SCF-deficient variant of the MCA26 model (32). Our data support and extend these observations by demonstrating that anti-KIT mAb treatment yields enhanced antitumor activity in combination with agents that target the clinically validated T-cell checkpoint proteins CTLA-4 and PD-1, and that these effects are associated with profoundly reduced M-MDSC numbers in both tumors and spleens of anti–KIT-treated mice. The reduction of M-MDSC numbers following anti-KIT mAb treatment is of further interest in light of the observation that, in melanoma patients treated with the immune checkpoint inhibitors ipilimumab or nivolumab, high numbers of circulating M-MDSCs were associated with lower survival benefit (25, 26). This suggests that targeting M-MDSCs through potent and selective inhibition of KIT may represent a novel combination strategy to enhance the efficacy of these immune checkpoint inhibitors. In addition, the reversal of the tumor-induced reduction in $CD4^+$ and $CD8^+$ T-cell numbers in splenocytes of anti–KIT-treated mice demonstrates that therapeutic targeting of KIT has the potential to promote antitumor responses via directly or indirectly influencing multiple immune cell types.

The precise mechanism whereby inhibition of KIT enhances the antitumor efficacy of immune checkpoint inhibitors is unclear, as is the mechanism whereby KIT inhibition reduces the MDSC population in tumor-bearing animals, and these are active areas of ongoing research. It is reported that mouse MDSCs do not themselves express detectable KIT protein (53), and we have confirmed by flow cytometry analysis that the M-MDSCs identified during these studies lack detectable KIT expression (data not shown), suggesting that the effect of anti-KIT treatment on M-MDSCs is likely to be indirect via modulation of a KIT-expressing cell type. Interactions between innate immune cells such as MDSCs and mast cells have been reported previously in various model systems (27, 28), and genetic studies in mice have also demonstrated that mast cells can exert strong immunosuppressive effects (29), implicating mast cells as a candidate KIT-expressing cell type mediating this effect. Unlike the majority of hematopoietic cell types, mature mast cells continue to express high levels of KIT and are functionally responsive to SCF for cell survival, cell migration, and secretion of a variety of inflammatory mediators including cytokines, lipid mediators, and proteases (54–56). The secretion of SCF by many tumor types provides a potential general mechanism of mast cell–dependent immunosuppression, whereby the tumor-secreted SCF triggers mast cell mediator release, thereby influencing the function of other cell types, including M-MDSCs, to generate an immunosuppressed environment supporting tumor growth. Selective inhibition of mast

cell KIT with a mAb, resulting in reduced MDSC function, would then be expected to reverse this tumor-induced immunosuppression, resulting in enhanced sensitivity to immuno-oncology agents including immune checkpoint inhibitors. Our data suggest that inhibitory mAbs targeting human KIT, such as KTN0158, have the potential to impact the immune environment in a variety of tumor types, providing support for future clinical evaluation of KTN0158 in combination with anti–PD-1, anti–PDL-1, and/or anti–CTLA-4 antibodies for the treatment of cancer.

Disclosure of Potential Conflicts of Interest

No potential conflicts of interest were disclosed.

Authors' Contributions

Conception and design: A.J. Garton, E.S. Trombetta, T.M. LaVallee, R. Gedrich
Development of methodology: L. Lopresti-Morrow, S. Mandiyan, S. Pankratz, T.M. LaVallee, R. Gedrich
Acquisition of data (provided animals, acquired and managed patients, provided facilities, etc.): S. Seibel, L. Lopresti-Morrow, L. Crew, N. Janson, S. Mandiyan, S. Pankratz, R. Gedrich
Analysis and interpretation of data (e.g., statistical analysis, biostatistics, computational analysis): A.J. Garton, S. Seibel, L. Lopresti-Morrow, S. Mandiyan, E.S. Trombetta, S. Pankratz, T.M. LaVallee, R. Gedrich
Writing, review, and/or revision of the manuscript: A.J. Garton, S. Seibel, L. Lopresti-Morrow, S. Mandiyan, E.S. Trombetta, T.M. LaVallee, R. Gedrich
Study supervision: E.S. Trombetta, T.M. LaVallee

Acknowledgments

The authors would like to thank Amos Brooks and Veronique Neumeister (Yale Pathology Tissue Services) for immunohistochemistry analysis of tumor samples.

The costs of publication of this article were defrayed in part by the payment of page charges. This article must therefore be hereby marked *advertisement* in accordance with 18 U.S.C. Section 1734 solely to indicate this fact.

Received October 13, 2016; revised December 15, 2016; accepted December 16, 2016; published OnlineFirst January 30, 2017.

References

1. Schlessinger J. Cell signaling by receptor tyrosine kinases. Cell 2000;103:211–25.
2. Yuzawa S, Opatowsky Y, Zhang Z, Mandiyan V, Lax I, Schlessinger J. Structural basis for activation of the receptor tyrosine kinase KIT by stem cell factor. Cell 2007;130:323–34.
3. Ullrich A, Schlessinger J. Signal transduction by receptors with tyrosine kinase activity. Cell 1990;61:203–12.
4. Reshetnyak AV, Nelson B, Shi X, Boggon TJ, Pavlenco A, Mandel-Bausch EM, et al. Structural basis for KIT receptor tyrosine kinase inhibition by antibodies targeting the D4 membrane-proximal region. Proc Natl Acad Sci U S A 2013;110:17832–7.
5. Miettinen M, Lasota J. KIT (CD117): a review on expression in normal and neoplastic tissues, and mutations and their clinicopathologic correlation. Appl Immunohistochem Mol Morphol 2005;13:205–20.
6. Heinrich MC, Corless CL, Demetri GD, Blanke CD, von Mehren M, Joensuu H, et al. Kinase mutations and imatinib response in patients with metastatic gastrointestinal stromal tumor. J Clin Oncol 2003;21:4342–9.
7. Goodman VL, Rock EP, Dagher R, Ramchandani RP, Abraham S, Gobburu JV, et al. Approval summary: sunitinib for the treatment of imatinib refractory or intolerant gastrointestinal stromal tumors and advanced renal cell carcinoma. Clin Cancer Res 2007;13:1367–73.
8. George S, Wang Q, Heinrich MC, Corless CL, Zhu M, Butrynski JE, et al. Efficacy and safety of regorafenib in patients with metastatic and/or unresectable GI stromal tumor after failure of imatinib and sunitinib: a multicenter phase II trial. J Clin Oncol 2012;30:2401–7.
9. Krug LM, Crapanzano JP, Azzoli CG, Miller VA, Rizvi N, Gomez J, et al. Imatinib mesylate lacks activity in small cell lung carcinoma expressing c-kit protein: a phase II clinical trial. Cancer 2005;103:2128–31.
10. Carvajal RD, Antonescu CR, Wolchok JD, Chapman PB, Roman RA, Teitcher J, et al. KIT as a therapeutic target in metastatic melanoma. JAMA 2011;305:2327–46.
11. Banat GA, Tretyn A, Pullamsetti SS, Wilhelm J, Weigert A, Olesch C, et al. Immune and inflammatory cell composition of human lung cancer stroma. PLoS One 2015;10:e0139073.
12. Ribatti D, Ennas MG, Vacca A, Ferreli F, Nico B, Orru S, et al. Tumor vascularity and tryptase-positive mast cells correlate with a poor prognosis in melanoma. Eur J Clin Invest 2003;33:420–5.
13. Yano H, Kinuta M, Tateishi H, Nakano Y, Matsui S, Monden T, et al. Mast cell infiltration around gastric cancer cells correlates with tumor angiogenesis and metastasis. Gastric Cancer 1999;2:26–32.
14. Fleischmann A, Schlomm T, Kollermann J, Sekulic N, Huland H, Mirlacher M, et al. Immunological microenvironment in prostate cancer: high mast cell densities are associated with favorable tumor characteristics and good prognosis. Prostate 2009;69:976–81.
15. Stahl M, Gedrich R, Peck R, LaVallee T, Eder JP. Targeting KIT on innate immune cells to enhance the antitumor activity of checkpoint inhibitors. Immunotherapy 2016;8:767–74.
16. Coussens LM, Raymond WW, Bergers G, Laig-Webster M, Behrendtsen O, Werb Z, et al. Inflammatory mast cells up-regulate angiogenesis during squamous epithelial carcinogenesis. Genes Dev 1999;13:1382–97.
17. Gounaris E, Erdman SE, Restaino C, Gurish MF, Friend DS, Gounari F, et al. Mast cells are an essential hematopoietic component for polyp development. Proc Natl Acad Sci U S A 2007;104:19977–82.
18. Soucek L, Lawlor ER, Soto D, Shchors K, Swigart LB, Evan GI. Mast cells are required for angiogenesis and macroscopic expansion of Myc-induced pancreatic islet tumors. Nat Med 2007;13:1211–8.
19. Wedemeyer J, Galli SJ. Decreased susceptibility of mast cell-deficient Kit (W)/Kit(W-v) mice to the development of 1, 2-dimethylhydrazine-induced intestinal tumors. Lab Invest 2005;85:388–96.
20. Oldford SA, Marshall JS. Mast cells as targets for immunotherapy of solid tumors. Mol Immunol 2015;63:113–24.
21. Postow MA, Callahan MK, Wolchok JD. Immune checkpoint blockade in cancer therapy. J Clin Oncol 2015;33:1974–82.
22. McDermott D, Haanen J, Chen TT, Lorigan P, O'Day S. Efficacy and safety of ipilimumab in metastatic melanoma patients surviving more than 2 years following treatment in a phase III trial (MDX010-20). Ann Oncol 2013;24:2694–8.
23. Gettinger SN, Horn L, Gandhi L, Spigel DR, Antonia SJ, Rizvi NA, et al. Overall survival and long-term safety of nivolumab (Anti-Programmed Death 1 Antibody, BMS-936558, ONO-4538) in patients with previously treated advanced non-small-cell lung cancer. J Clin Oncol 2015;33:2004–12.
24. Economopoulou P, Perisanidis C, Giotakis EI, Psyrri A. The emerging role of immunotherapy in head and neck squamous cell carcinoma (HNSCC): anti-tumor immunity and clinical applications. Ann Transl Med 2016;4:173.
25. Kitano S, Postow MA, Ziegler CG, Kuk D, Panageas KS, Cortez C, et al. Computational algorithm-driven evaluation of monocytic myeloid-derived suppressor cell frequency for prediction of clinical outcomes. Cancer Immunol Res 2014;2:812–21.
26. Weber J, Gibney G, Kudchadkar R, Yu B, Cheng P, Martinez AJ, et al. Phase I/II study of metastatic melanoma patients treated with nivolumab who had progressed after ipilimumab. Cancer Immunol Res 2016;4:345–53.
27. Saleem SJ, Martin RK, Morales JK, Sturgill JL, Gibb DR, Graham L, et al. Cutting edge: mast cells critically augment myeloid-derived suppressor cell activity. J Immunol 2012;189:511–5.
28. Danelli L, Frossi B, Gri G, Mion F, Guarnotta C, Bongiovanni L, et al. Mast cells boost myeloid-derived suppressor cell activity and contribute to the development of tumor-favoring microenvironment. Cancer Immunol Res 2015;3:85–95.

29. Wasiuk A, Dalton DK, Schpero WL, Stan RV, Conejo-Garcia JR, Noelle RJ. Mast cells impair the development of protective anti-tumor immunity. Cancer Immunol Immunother 2012;61:2273–82.
30. Ozao-Choy J, Ma G, Kao J, Wang GX, Meseck M, Sung M, et al. The novel role of tyrosine kinase inhibitor in the reversal of immune suppression and modulation of tumor microenvironment for immune-based cancer therapies. Cancer Res 2009;69:2514–22.
31. Christiansson L, Soderlund S, Mangsbo S, Hjorth-Hansen H, Hoglund M, Markevarn B, et al. The tyrosine kinase inhibitors imatinib and dasatinib reduce myeloid suppressor cells and release effector lymphocyte responses. Mol Cancer Ther 2015;14:1181–91.
32. Pan PY, Wang GX, Yin B, Ozao J, Ku T, Divino CM, et al. Reversion of immune tolerance in advanced malignancy: modulation of myeloid-derived suppressor cell development by blockade of stem-cell factor function. Blood 2008;111:219–28.
33. Kalesnikoff J, Galli SJ. Antiinflammatory and immunosuppressive functions of mast cells. Methods Mol Biol 2011;677:207–20.
34. Iwaki S, Tkaczyk C, Satterthwaite AB, Halcomb K, Beaven MA, Metcalfe DD, et al. Btk plays a crucial role in the amplification of Fc epsilonRI-mediated mast cell activation by kit. J Biol Chem 2005;280:40261–70.
35. Kuehn HS, Radinger M, Gilfillan AM. Measuring mast cell mediator release. Curr Protoc Immunol 2010;Chapter 7:Unit7 38.
36. Lev S, Blechman J, Nishikawa S, Givol D, Yarden Y. Interspecies molecular chimeras of kit help define the binding site of the stem cell factor. Mol Cell Biol 1993;13:2224–34.
37. Coleman JW, Holliday MR, Kimber I, Zsebo KM, Galli SJ. Regulation of mouse peritoneal mast cell secretory function by stem cell factor, IL-3 or IL-4. J Immunol 1993;150:556–62.
38. Manley PW, Drueckes P, Fendrich G, Furet P, Liebetanz J, Martiny-Baron G, et al. Extended kinase profile and properties of the protein kinase inhibitor nilotinib. Biochim Biophys Acta 2010;1804:445–53.
39. Verstovsek S, Akin C, Manshouri T, Quintas-Cardama A, Huynh L, Manley P, et al. Effects of AMN107, a novel aminopyrimidine tyrosine kinase inhibitor, on human mast cells bearing wild-type or mutated codon 816 c-kit. Leuk Res 2006;30:1365–70.
40. Grosso JF, Jure-Kunkel MN. CTLA-4 blockade in tumor models: an overview of preclinical and translational research. Cancer Immun 2013;13:5.
41. Huang B, Lei Z, Zhang GM, Li D, Song C, Li B, et al. SCF-mediated mast cell infiltration and activation exacerbate the inflammation and immunosuppression in tumor microenvironment. Blood 2008;112:1269–79.
42. Rigoni A, Colombo MP, Pucillo C. The role of mast cells in molding the tumor microenvironment. Cancer Microenviron 2015;8:167–76.
43. Walunas TL, Lenschow DJ, Bakker CY, Linsley PS, Freeman GJ, Green JM, et al. CTLA-4 can function as a negative regulator of T cell activation. Immunity 1994;1:405–13.
44. Yamazaki T, Akiba H, Koyanagi A, Azuma M, Yagita H, Okumura K. Blockade of B7-H1 on macrophages suppresses CD4+ T cell proliferation by augmenting IFN-gamma-induced nitric oxide production. J Immunol 2005;175:1586–92.
45. Parker KH, Beury DW, Ostrand-Rosenberg S. Myeloid-derived suppressor cells: critical cells driving immune suppression in the tumor microenvironment. Adv Cancer Res 2015;128:95–139.
46. Ebos JM, Lee CR, Christensen JG, Mutsaers AJ, Kerbel RS. Multiple circulating proangiogenic factors induced by sunitinib malate are tumor-independent and correlate with antitumor efficacy. Proc Natl Acad Sci U S A 2007;104:17069–74.
47. Wang CH, Anderson N, Li SH, Szmitko PE, Cherng WJ, Fedak PW, et al. Stem cell factor deficiency is vasculoprotective: unraveling a new therapeutic potential of imatinib mesylate. Circ Res 2006;99:617–25.
48. Porembka MR, Mitchem JB, Belt BA, Hsieh CS, Lee HM, Herndon J, et al. Pancreatic adenocarcinoma induces bone marrow mobilization of myeloid-derived suppressor cells which promote primary tumor growth. Cancer Immunol Immunother 2012;61:1373–85.
49. Wesolowski R, Markowitz J, Carson WE 3rd. Myeloid derived suppressor cells - a new therapeutic target in the treatment of cancer. J Immunother Cancer 2013;1:10.
50. Draghiciu O, Nijman HW, Hoogeboom BN, Meijerhof T, Daemen T. Sunitinib depletes myeloid-derived suppressor cells and synergizes with a cancer vaccine to enhance antigen-specific immune responses and tumor eradication. Oncoimmunology 2015;4:e989764.
51. Larmonier N, Janikashvili N, LaCasse CJ, Larmonier CB, Cantrell J, Situ E, et al. Imatinib mesylate inhibits CD4+ CD25+ regulatory T cell activity and enhances active immunotherapy against BCR-ABL- tumors. J Immunol 2008;181:6955–63.
52. Balachandran VP, Cavnar MJ, Zeng S, Bamboat ZM, Ocuin LM, Obaid H, et al. Imatinib potentiates antitumor T cell responses in gastrointestinal stromal tumor through the inhibition of Ido. Nat Med 2011;17:1094–100.
53. Talmadge JE, Gabrilovich DI. History of myeloid-derived suppressor cells. Nat Rev Cancer 2013;13:739–52.
54. Tsai M, Takeishi T, Thompson H, Langley KE, Zsebo KM, Metcalfe DD, et al. Induction of mast cell proliferation, maturation, and heparin synthesis by the rat c-kit ligand, stem cell factor. Proc Natl Acad Sci U S A 1991;88:6382–6.
55. Ito T, Smrz D, Jung MY, Bandara G, Desai A, Smrzova S, et al. Stem cell factor programs the mast cell activation phenotype. J Immunol 2012;188:5428–37.
56. Al-Azzam N, Kondeti V, Duah E, Gombedza F, Thodeti CK, Paruchuri S. Modulation of mast cell proliferative and inflammatory responses by leukotriene d4 and stem cell factor signaling interactions. J Cell Physiol 2015;230:595–602.